ORIGINAL RESEARCH

# Helicity and Vorticity of Pulmonary Arterial Flow in Patients With Pulmonary Hypertension: Quantitative Analysis of Flow Formations

Michal Schäfer, MSc; Alex J. Barker, PhD; Vitaly Kheyfets, PhD; Kurt R. Stenmark, MD; James Crapo, MD; Michael E. Yeager, PhD; Uyen Truong, MD; J. Kern Buckner, MD; Brett E. Fenster, MD;* Kendall S. Hunter, MD*

***Background*—**Qualitative and quantitative flow hemodynamic indexes have been shown to reflect right ventricular (RV) afterload and function in pulmonary hypertension (PH). We aimed to quantify flow hemodynamic formations in pulmonary arteries using 4-dimensional flow cardiac magnetic resonance imaging and the spatial velocity derivatives helicity and vorticity in a heterogeneous PH population.

***Methods and Results*—**Patients with PH (n=35) and controls (n=10) underwent 4-dimensional flow magnetic resonance imaging study for computation of helicity and vorticity in the main pulmonary artery (MPA), the right pulmonary artery, and the RV outflow tract. Helicity and vorticity were correlated with standard RV volumetric and functional indexes along with MPA stiffness assessed by measuring relative area change. Patients with PH had a significantly decreased helicity in the MPA (8 versus 32 $m/s^2$; $P<0.001$), the right pulmonary artery (24 versus 50 $m/s^2$; $P<0.001$), and the RV outflow tract–MPA unit (15 versus 42 $m/s^2$; $P<0.001$). Vorticity was significantly decreased in patients with PH only in the right pulmonary artery (26 versus 45 1/s; $P<0.001$). Total helicity computed correlated with the cardiac magnetic resonance imaging–derived ventricular-vascular coupling (−0.927; $P<0.000$), the RV ejection fraction (0.865; $P<0.0001$), cardiac output (0.581; $P<0.0001$), mean pulmonary arterial pressure (−0.581; $P=0.0008$), and relative area change measured at the MPA (0.789; $P<0.0001$).

***Conclusions*—**The flow hemodynamic character in patients with PH assessed via quantitative analysis is considerably different when compared with healthy and normotensive controls. A strong association between helicity in pulmonary arteries and ventricular-vascular coupling suggests a relationship between the mechanical and flow hemodynamic domains. **(*J Am Heart Assoc*. 2017;6:e007010. DOI: 10.1161/JAHA.117.007010.)**

**Key Words:** flow imaging • hemodynamics • magnetic resonance imaging • pulmonary hypertension

Noninvasive flow evaluation is an increasingly recognized component of pulmonary hypertension (PH) imaging, with wide research and clinical applications.[1,2] Qualitative and quantitative flow hemodynamic indexes have been shown to reflect right ventricular (RV) afterload and function, the 2 most important predictors of clinical outcomes.[3–5] Furthermore, flow hemodynamic forces are well-established mediators of vascular remodeling with the potential to augment proximal pulmonary vascular stiffness, an increasingly recognized theme in PH.[6–10] Although the clinical role of standard PH characteristics, including catheterization, RV specific size and functional metrics, and PH specific clinical markers, has been already established, only a limited amount of studies have focused on flow characterization in PH.[11,12]

Four-dimensional flow cardiac magnetic resonance imaging (MRI; 4D-Flow CMR) is the most common modality for comprehensive spatial flow evaluation with the ability to accurately assess the 3-dimensional (3D) hemodynamic changes within any anatomical compartment of interest.[13] Specifically, 4D-Flow MRI enables qualitative analysis of pulmonary flow, which is known in PH to form into chaotic, turbulent, and energy dissipative formations.[3,14–16] Vascular flow formations described in helical and vortical patterns have in the past been associated with regional propensity to overt

*From the Divisions of Cardiology (M.S., U.T., J.K.B., B.E.F., K.S.H.) and Pulmonary Medicine (J.C.), National Jewish Health, Denver, CO; Division of Cardiology, Children's Hospital Colorado, Aurora, CO (M.S.); Department of Bioengineering (M.S., V.K., K.R.S., M.E.Y., U.T., K.S.H.) and Pediatric Division, Department of Critical Care and Pulmonary Medicine (K.R.S.), University of Colorado Denver | Anschutz Medical Campus, Denver, CO; and Department of Radiology, Feinberg School of Medicine, Northwestern University, Chicago, IL (A.J.B.).*

An accompanying Figure S1 is available at http://jaha.ahajournals.org/content/6/12/e007010/DC1/embed/inline-supplementary-material-1.pdf

*Dr Fenster and Dr Hunter are co-senior authors.

**Correspondence to:** Michal Schäfer, MSc, Department of Cardiology, Children's Hospital Colorado, 13123 E 16th Ave, Aurora, CO 80045-2560. E-mail: michal.schafer@ucdenver.edu

Received June 21, 2017; accepted September 29, 2017.

## Clinical Perspective

### What Is New?

- Flow hemodynamic formations in patients with pulmonary hypertension are quantitatively significantly different from those in normotensive controls and are associated with ventricular-vascular coupling, suggesting an association between flow energy dissipation and vascular afterload.

### What Are the Clinical Implications?

- Noninvasive evaluation of patients with pulmonary hypertension via 4-dimensional flow cardiac magnetic resonance imaging offers comprehensive assessment of flow hemodynamics and characterization with respect to ventricular function and proximal pulmonary vascular stiffness.
- Quantitative evaluation of the hemodynamic flow condition might be more reflective of pulmonary hypertension severity than qualitative grading and might serve as a diagnostic screening tool for pulmonary hypertension before or in addition to initial catheterization evaluation.

vascular remodeling toward collagen-based character, inflammation, and dilation features, commonly leading to augmentation of vascular stiffness.[17–20] Indeed, in our previous investigations, we have described reduced main pulmonary arterial (MPA) compliance and distensibility in association with reduced hemodynamic shear stress and increased flow recirculation in both adult and pediatric PH populations.[14,21] However, 3D macroscopic flow formations are preferably qualitatively evaluated using custom scales and are difficult to normalize to the size and function of particular cardiovascular anatomy. In addition, the low temporal resolution typically associated with 4D-Flow CMR data sets disables more discrete qualitative evaluation. Therefore, in this study, we aimed to quantify flow hemodynamic formations in proximal pulmonary arteries using 4D-Flow CMR and the spatial velocity derivatives helicity and vorticity in a heterogeneous patient population with PH. We hypothesized that vorticity and helicity metrics will significantly differ in patients with PH from those in healthy controls and that both metrics will be reflective of pulmonary arterial stiffness and RV function. The better understanding of the flow hemodynamics and their association with pulmonary vascular stiffness in PH may lead to a better understanding of the pathophysiological processes through the course of the disease and to the identification of novel therapeutic targets.

## Methods

### Study Population

As a part of a prospective study, patients with diagnosed PH (n=35) and normal controls (n=10) underwent an institutional review board–approved 4D-Flow MRI study. PH was defined as mean pulmonary artery pressure ≥25 mm Hg, determined by initial right-sided heart catheterization, as previously described.[5] The idiopathic pulmonary arterial hypertension group (class I) was defined as main pulmonary arterial pressure (mPAP) >25 mm Hg and pulmonary arterial wedge pressure ≤15 mm Hg. PH attributable to the chronic lung disease group (class III) was defined as mPAP >25 mm Hg, predicted forced expiratory volume in a second <60%, and predicted functional vital capacity <70%. Furthermore, all class III patients had computed tomography–confirmed characteristic airway and parenchymal abnormalities. Included patients had no history of cardiovascular surgery, arrhythmia, or myocardial ischemia, and were without any evidence of congenital lesions. The ventricular distress molecules, brain natriuretic peptide and NT-proBNP (N-terminal pro-B-type BNP), were collected at catheterization, as indicated by clinical care. All control subjects were without history of cardiovascular disease. Informed consent was obtained in all subjects.

### Cardiac Magnetic Resonance

CMR with the 4D-Flow technique was performed using a 1.5-T MRI Siemens system (MAGNETOM; Avanto, Erlangen, Germany) with an 8-channel phased array coil. The field of view was oriented to cover the entire mediastinum and great vessels. 4D-Flow CMR images were acquired using an radiofrequency-spoiled gradient echo pulse sequence, prospective electrocardiogram gating, and respiratory navigators using bellows with interleaved 3-directional velocity encoding. Depending on patient size and field of view, typical scanning parameters were as follows: spatial resolution, 2.4 to 2.6×2.4 to 2.6×2.4 to 3.0 mm; $\alpha$=14° to 15°; echo time/repetition time, 2.85/48.56 ms. Velocity-encoding values were adjusted according to the maximum velocities encountered during scout sequences to avoid aliasing artifact (typical values ranged from 100–150 cm/s). Resulting acquisition time varied on the basis of heart rate and respiratory gating efficiency from 15 to 25 minutes.

A cine steady-state free precession technique with retrospective gating was used to image the heart from the base to the apex during brief end-expiratory breath holds using contiguous short-axis slices in 8-mm increments. Ventricular volumetric and functional analyses, along with RV mass index assessment, were performed off line by a blinded reader using commercially available software (Argus, MR B17; Siemens AG Healthcare Sector, Erlangen, Germany). Ventricular end-diastolic and end-systolic contours were manually traced in the axial view for each slice. RV volumes and ejection fractions were then determined using the modified Simpson rule. In addition, the steady-state free precession images also

served for the assessment of MPA and right pulmonary artery (RPA) dimensions and the MPA relative area change (RAC) $\{[(A_{max}-A_{min})/A_{max}]\times 100$, where $A_{max}$ is maximum area, and $A_{min}$ is minimum area$\}$, which was computed 1 cm above the pulmonic valve. Last, the CMR-derived RV-specific ventricular/vascular coupling ratio (VVCR) was calculated, as shown previously, as a ratio of RV end-systolic and stroke volumes.[22]

## Quantification of Vorticity and Helicity and Qualitative Analysis

The raw 4D-Flow MRI data sets were preprocessed and corrected for phase offset errors, noise, and antialiasing, as described previously, using consensus recommendations.[13] The preprocessed 4D-Flow CMR data sets were then converted for quantitative and qualitative analysis (ParaView; Kitware, Clifton, NY) using a custom-made MATLAB program (Mathworks, Nattick, MA).[23] Vascular contours required for anatomical segmentation were created by conversion of the 4D-Flow MRI magnitude and phase-specific images into the 3D phase-contrast MRI angiography (MRA) domain, as shown previously.[24] Specifically, the MRA data set was created by multiplication of spatially respective magnitude and velocity images, described as follows:

$$I_i^{MRA}(\vec{r}) = I_i^{Mag}(\vec{r})\sqrt{\sum_{j=x,y,z} v_{i,j}^2(\vec{r})}$$

where $\vec{r}$ represents the spatial location within the 3D magnitude ($I^{Mag}$) and velocity (v) domains, i represents the cardiac phase, and j represents one of the principal velocity encoding direction (x, y, z).[24,25] Manual segmentation of the vascular compartments was achieved from constructed MRA using freely available software (ITK_snap; Kitware). Specific segments of the proximal pulmonary conduit undergoing helicity and vorticity evaluation were divided into 3 anatomically differentiated compartments (Figure 1). The MPA luminal region of interest was defined as the volume extending from the pulmonic valve to the distal end of the MPA bifurcation, using the planes that define the ostia of the right and left pulmonary artery as lateral boundaries. The RPA luminal portion was defined as the volume extending from the RPA ostial plane (MPA boundary) to planes that defined the ostia of the right middle and right lower lobar arteries. The RV outflow tract (RVOT) region of interest was defined as the volume enclosed by both the septal and free wall portions of the corresponding muscular rings, with crista supraventricularis serving as the most inferior boundary. As shown in previous velocity-encoding MRI limitations, our acquisition window captured a portion of the left pulmonary artery, but these regions were not uniform and complete in each case, mainly because of anatomical and size variations; therefore, the left pulmonary artery analysis was excluded from this study.[26]

Vorticity and helicity were analyzed from 4D-Flow CMR velocity vector fields in each temporal phase, using a bilinear

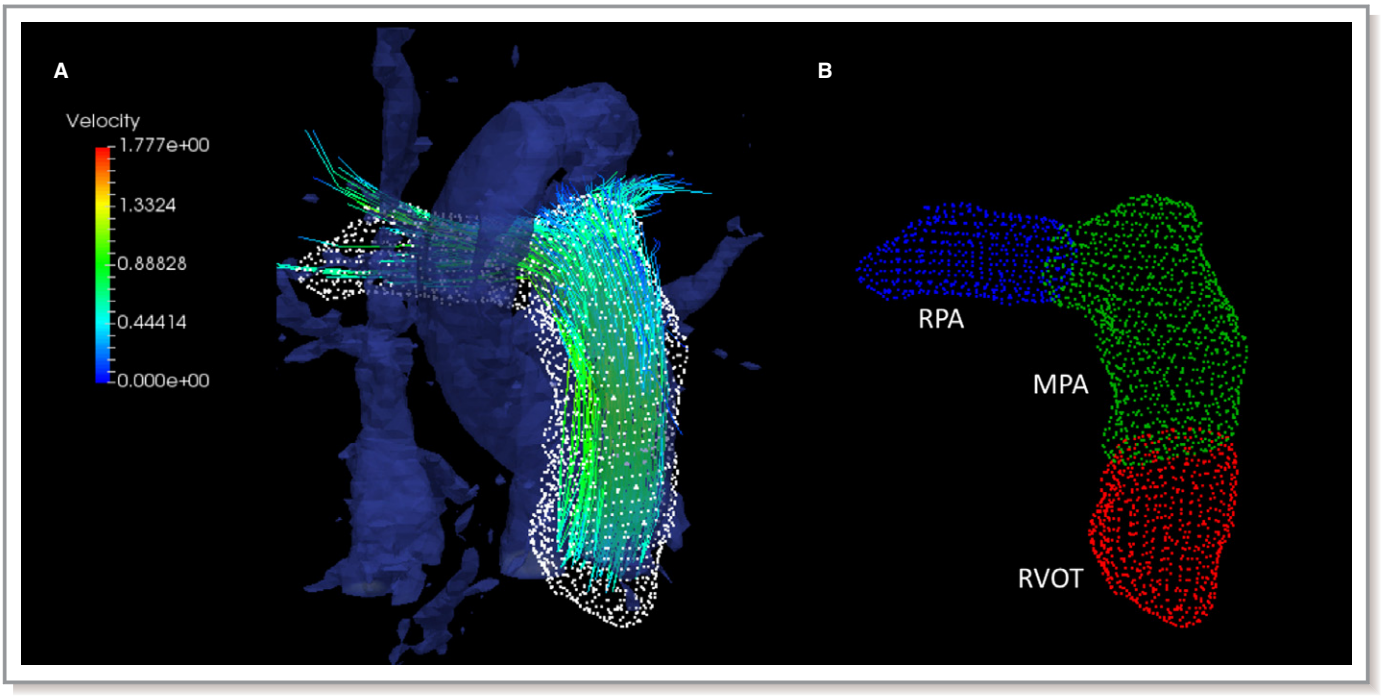


**Figure 1.** A, Streamline visualization of segmented proximal pulmonary arteries from 4-dimensional flow cardiac magnetic resonance imaging derived magnetic resonance angiography. B, The evaluated segments included the right ventricular outflow tract (RVOT), the main pulmonary artery (MPA), and the right pulmonary artery (RPA).

interpolation scheme over the entire anatomical region of interest defined by reconstructed 3D MRA. Vorticity is in mathematical terms a vector (the curl of the velocity field describing local flow rotation rate), defined precisely as follows:

$$\omega(x,t) = \nabla \times v(x,t)$$

where $\nabla$ represents the spatial derivative operator commonly known as nabla and $v(x,t)$ represents the velocity measured at any time point t of the cardiac cycle at defined anatomical location x. We then calculated the magnitude of vorticity, which was spatially integrated using the cumulative sum function and multiplied by voxel volume to provide the corresponding integral, as shown previously.[27–29] Visually, the relationship between the magnitude velocity and vorticity vector fields can be easily seen in Figure 2, showing that velocity streamlines with the vorticity vector field, typically delineating the endothelial boundary. Vascular region-specific vorticity was then computed and sampled, as shown previously, with vorticity being measured along the entire predefined pulmonary vascular domain (MPA-RVOT, MPA, and RPA), with maximum systolic vorticity being sampled from the vorticity waveform for comparative analysis, as shown in Figure 2.[4,29]

Quantification of helicity has previously been successfully described in systemic circulation using both computational modeling and 4D-Flow CMR.[18,19,30,31] Unlike vorticity, helicity is a scalar describing the relationship between flow strength and the amount of local rotation in flow-vorticity, and reflects on stability of laminar flow and propensity toward developing turbulent structures.[30,32,33] Mathematically, helicity is defined as follows:

$$H(x,t) = v(x,t) \cdot \omega(x,t)$$

and similar to vorticity, it can be visualized as a scalar field at any time and position in the cardiovascular region of interest (Figure 3). Maximum systolic helicity was then collected from the helicity waveform computed in predefined regions, as described in the vorticity quantification process.

## Statistical Analysis

Analyses were performed using JMP Pro 13.0 (SAS Institute, Cary, NC). Variables were checked for the distributional assumption of normality using normal plots, in addition to Kolmogorov-Smirnov and Shapiro-Wilks tests. All normally distributed group-specific data sets are reported as means

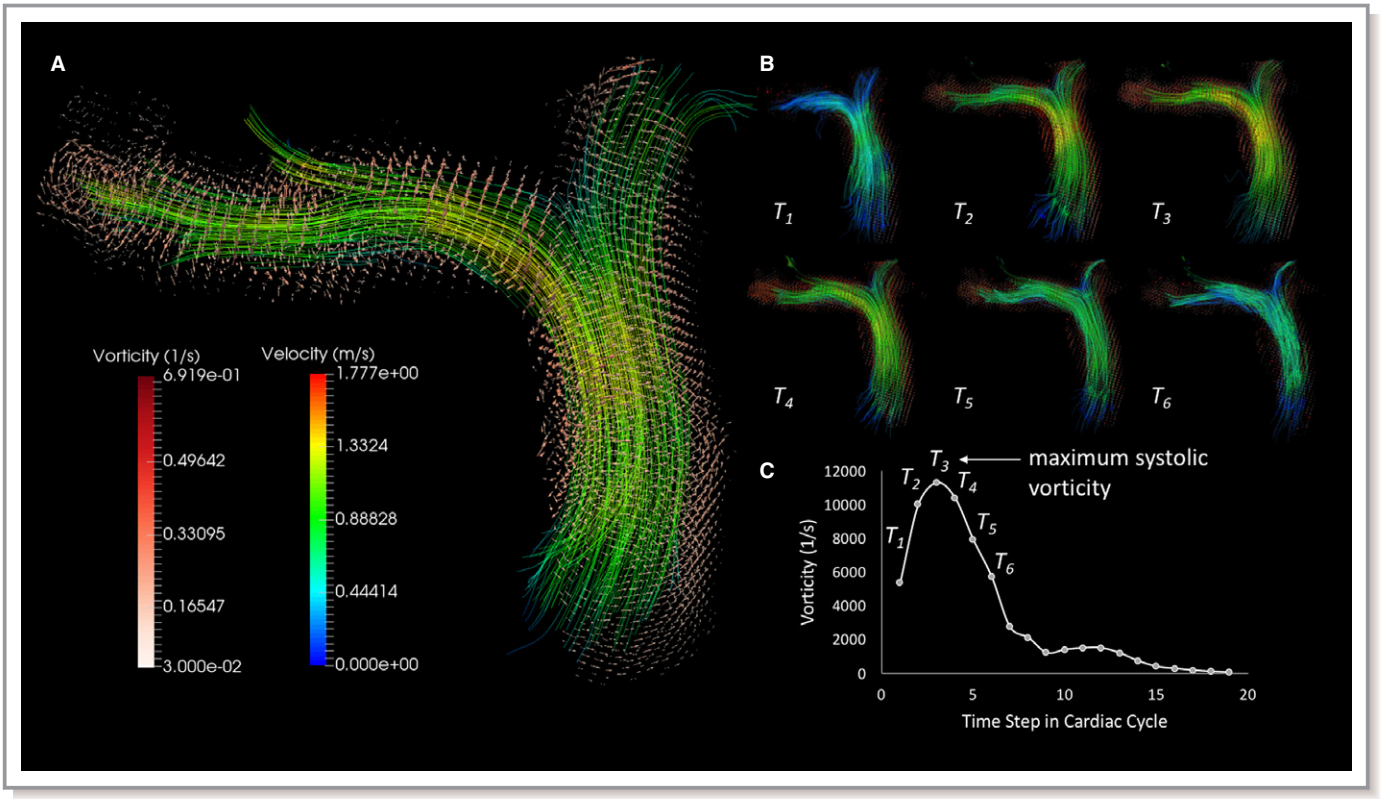


**Figure 2.** Vorticity visualization and quantification. A, Velocity streamlines in proximal pulmonary conduit vessels with superimposed vorticity vector field delineating the arterial luminal surface. B, Evolution of velocity and vorticity in pulmonary arteries in the systolic phase of the cardiac cycle. C, Reconstructed vorticity waveform has a similar shape to the classic flow curve with maximum systolic vorticity sampled in each case.

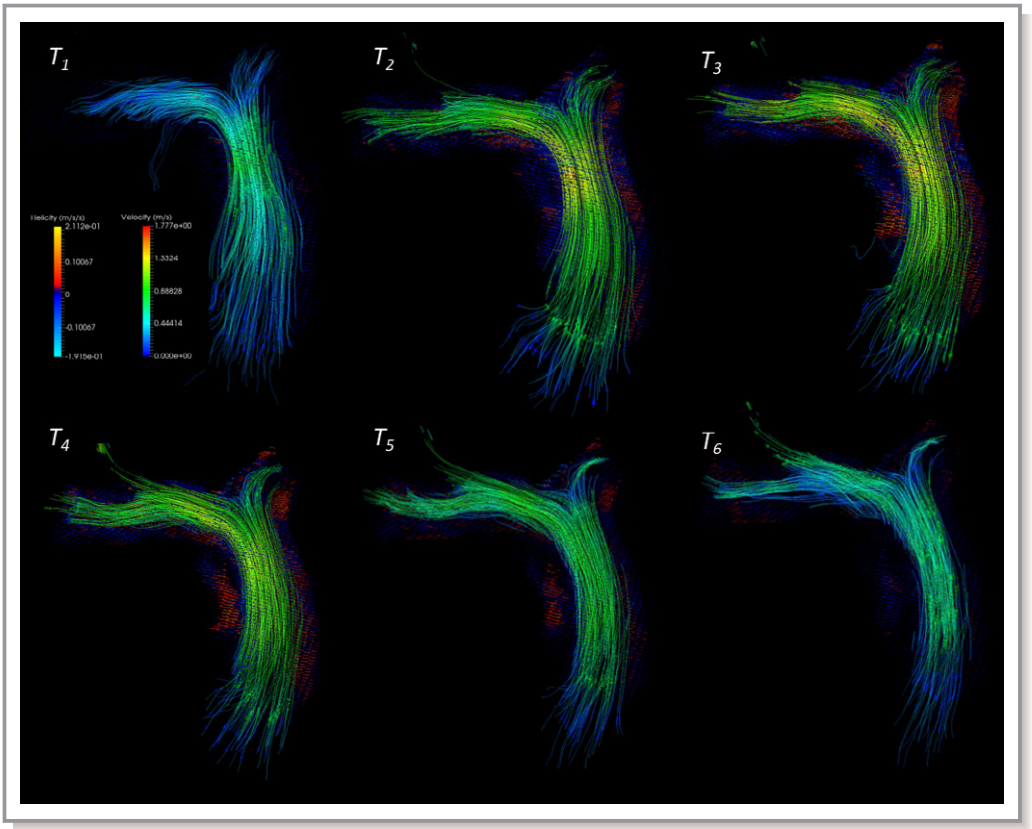


**Figure 3.** Visualization of helicity field along the pulmonary arterial tracts herein depicted in a healthy control subject. Maximum helicity was then calculated similarly as vorticity from the generated helicity waveform.

with corresponding SDs or as median values with interquartile ranges if nonuniformly distributed. Demographic and clinical characteristics among patients with PH and controls were compared using a Student 2-sided *t* test for normally distributed continuous variables, a Wilcoxon ranked sum test for nonuniform distributed variables, and a $\chi^2$ test for categorical variables. Simple linear regressions were evaluated using the Pearson *R* (eg, helicity versus MPA RAC, cardiac output, and mPAP) and nonlinear regressions using the Spearman ρ (eg, helicity versus VVCR) to ensure the best fit (power series was applied for nonlinear relationships) and to evaluate the associations between helicity and vorticity metrics and known PH risk predictors and steady-state free precession measures (eg, RV ejection fraction, mPAP, and VVCR). The intraclass correlation coefficient (ICC) along with Bland-Altman analysis was used to assess interobserver and intraobserver variabilities for helicity measurement. Intraobserver and interobserver variabilities of helicity measurements were assessed separately in 10 randomly selected patients with PH and in all control subjects. The RVOT-MPA region was selected for this analysis because of highly variable anatomical features and large volume coverage. Intraobserver variability was based on measurements by the same observer (M.S.) at different times (6 months apart). Last, the diagnostic sensitivity and specificity of 4D-Flow-derived indexes were assessed by receiver operating characteristic curve, with the Youden index being applied to find specific cutoff values. Significance was based on an α-level of 0.05.

## Results

Demographic and basic hemodynamic characteristics are summarized in Table 1. The average time between the right-sided heart catheterization and 4D-Flow MRI was 76 days (range, 0–591 days). The average mean pulmonary arterial pressure and pulmonary vascular resistance from chronologically closest catheterization were 36±11 mm Hg and 8.5±6.4 Wood units. There were 16 patients with idiopathic PH (class I), 16 patients with PH attributable to chronic lung disease (class III), and 3 patients with unclear or multifactorial disease mechanisms (class V), as per PH consensus classification.[5] All included patients with PH (n=35) and control subjects (n=10) underwent successful 4D-Flow MRI acquisition.

As anticipated, patients with PH had elevated RV end-diastolic (165 versus 112 mL; $P<0.0011$) and end-systolic

**Table 1.** Patient Characteristics

| Characteristics | PH Group (n=35) | Control Group (n=10) | *P* Value |
|---|---|---|---|
| Age, y | 61±9 | 57±9 | 0.3092 |
| Female sex, n (%) | 21 (60) | 7 (70) | . . . |
| BSA, $m^2$ | 1.79±0.24 | 1.87±0.25 | 0.3979 |
| mPAP, mm Hg | 36.4±11.0 | . . . | . . . |
| PVR, WU | 8.5±6.4 | . . . | . . . |
| PAWP, mm Hg | 11.7±3.9 | . . . | . . . |
| WHO classification, n (%) | | | |
| Class I | 16 (46) | . . . | . . . |
| Class III | 16 (46) | . . . | . . . |
| Class V | 3 (8) | . . . | . . . |
| 6-MWT | 328±96 | . . . | . . . |
| NT-proBNP, ng/L | 420 (243–1879) | . . . | . . . |
| BNP, ng/L | 44 (16–122) | . . . | . . . |
| RVEDV, mL | 165±68 | 112±28 | 0.0011 |
| RVESV, mL | 101±68 | 46±15 | <0.0001 |
| RVSV, mL | 63±20 | 66±16 | 0.6230 |
| RV mass index, $g/m^2$ | 34±11 | 16±7 | <0.0001 |
| RVEF, % | 43±15 | 59±5 | <0.0001 |
| VVCR | 1.87±1.51 | 0.69±0.17 | <0.0001 |
| RVCO, L/min | 3.5±1.4 | 3.7±0.8 | 0.4278 |
| HR, bpm | 54±18 | 57±7 | 0.5203 |
| MPA $V_{max}$, m/s | 0.61±0.24 | 0.82±0.26 | <0.0001 |
| RPA $V_{max}$, m/s | 0.58±0.21 | 0.85±0.13 | <0.0001 |
| MPA size, cm | 3.5±0.4 | 2.3±0.4 | <0.0001 |
| RPA size, cm | 2.5±0.4 | 1.7±0.2 | <0.0001 |
| MPA RAC, % | 29±5 | 16±5 | <0.0001 |

Data are reported as mean±SD or median (interquartile range) unless otherwise indicated. 6-MWT indicates 6-minute walk test; BNP, brain natriuretic peptide; BSA, body surface area; HR, heart rate; MPA, main pulmonary artery; mPAP, main pulmonary arterial pressure; NT-proBNP, N-terminal pro-B-type BNP; PAWP, pulmonary arterial wedge pressure; PH, pulmonary hypertension; PVR, pulmonary vascular resistance; RAC, relative area change; RPA, right pulmonary artery; RV, right ventricular; RVCO, RV cardiac output; RVEDV, RV end-diastolic volume; RVEF, RV ejection fraction; RVESV, RV end-systolic volume; RVSV, RV stroke volume; $V_{max}$, maximum velocity; VVCR, ventricular/vascular coupling ratio; WHO, World Health Organization; and WU, Wood unit.

(101 versus 46 mL; *P*<0.0001) volumes, with reduced RV ejection fraction (43% versus 59%; *P*<0.0001) and significantly elevated VVCR (1.87 versus 0.69; *P*<0.0001). RV mass index was significantly elevated in the PH group when compared with controls (34 versus 11 $g/m^2$; *P*<0.0001). The PH group had further elevated maximum MPA (3.5 versus 2.3 cm; *P*<0.0001) and RPA (2.5 versus 1.7 cm; *P*<0.0001) diameters. Correspondingly, the maximum velocity measured in the MPA was decreased in the PH group (0.61 versus 0.82 m/s; *P*<0.0001), with a similar finding in the RPA (0.58 versus 0.85 m/s; *P*<0.0001). The RAC measured in the MPA was significantly reduced in patients with PH (16% versus 29%; *P*<0.0001), indicative of increased MPA stiffness in this heterogeneous PH population.

Table 2 shows a summary of 4D-Flow derived flow quantitative indexes further graphically depicted in Figure 4. Helicity was significantly reduced in patients with PH in both the MPA (8 versus 32 $m/s^2$; *P*=0.0002) and the RPA (50 versus 24 $m/s^2$; *P*<0.0001). The helicity was significantly depressed in the MPA in the PH group, even when combined with the RVOT (15 versus 42 $m/s^2$; *P*=0.0003) and when summarized in all considered regions (46 versus 92 $m/s^2$; *P*<0.0001). On the other hand, no significant difference existed between vorticity measured in the MPA (1562 versus 1565 1/s; *P*=0.9682) or within the MPA-RVOT (2084 versus 2244 1/s; *P*=0.4074). However, vorticity measured in the RPA was significantly decreased in the population with PH (2600 versus 4490 [1/s]; *P*=0.0002) and when summed along all considered anatomical regions (6020 versus 8560 [1/s]; *P*=0.0022). No variability existed between different PH classes in total helicity (*P*=0.9945) and vorticity (*P*=0.4875) metrics. Subanalysis considering standard CMR functional and volumetric indexes and 4D-Flow metrics between class I and class III PH groups (both n=16) did not reveal any significant differences.

The interobserver analysis for the helicity assessment in MPA-RVOT region revealed good agreement in both PH (ICC, 0.94; mean difference, 0.4; 95% confidence interval, −2.0 to 2.8) and control (ICC, 0.99; mean difference, −0.4; 95% confidence interval, −1.4 to 0.7) groups. Similarly, the intraobserver analysis performed 6 months apart showed strong agreement in PH (ICC, 0.98; mean difference, 0.3; 95% confidence interval, −0.8 to 1.5) and control (ICC, 0.99; mean difference, 1.1; 95% confidence interval, 0.6–1.6) groups. The corresponding Bland-Altman plots are portrayed in Figure S1.

To investigate the relationship between the quantitative flow hemodynamic metrics and the markers of RV function and afterload, we performed correlative analysis between total helicity and vorticity with the steady-state free precession–derived RV and vascular measures. A summary of all performed correlations (reported as *R* or ρ value with corresponding *P* value) is depicted in Table 3. Total helicity had a strong negative curvilinear correlation with the VVCR ($\rho$=−0.916; *P*<0.0001), end-systolic volume (*R*=−0.482; *P*=0.0008), and end-diastolic volume (*R*=−0.472; *P*=0.0010). In addition, helicity positively correlated with the RV ejection fraction (*R*=0.865; *P*<0.0001), RV stroke volume (*R*=0.477; *P*=0.0009), and cardiac output (*R*=0.581; *P*<0.0001). Furthermore, total helicity negatively correlated with mPAP (*R*=−0.581; *P*=0.0008) and positively correlated with the RAC measured in the MPA (*R*=0.789; *P*<0.0001). The

**Table 2.** Vorticity and Helicity

| Variable | Helicity ($m/s^2$) | | Vorticity (1/s) (×100) | |
|---|---|---|---|---|
| | PH Group (n=35) | Control Group (n=10) | PH Group (n=35) | Control Group (n=10) |
| MPA | 8 (6–17) | 32 (21–35)* | 13.4 (11.9–18.7) | 14.8 (13.3–16.9) |
| RVOT+MPA | 15 (11–34) | 42 (40–48)* | 20.0 (16.0–23.9) | 21.7 (19.0–24.1) |
| RPA | 24 (15–33) | 50 (42–57)* | 26.0 (17.2–31.2) | 44.9 (42.7–54.5)* |
| Total | 46 (27–66) | 92 (86–98)* | 60.2 (49.5–71.6) | 85.6 (76.5–92.8)* |

Data are reported as median (interquartile range). MPA indicates main pulmonary artery; PH, pulmonary hypertension; RPA, right pulmonary artery; and RVOT, right ventricular outflow tract.
*$P<0.05$.

significant correlations between helicity and RV afterload/function indexes are depicted in Figure 5. Total vorticity showed comparatively weaker correlations with the same markers as helicity. A significant negative correlation existed between total vorticity and the VVCR ($\rho=-0.426$; $P=0.0058$), whereas a positive correlation was observed with the RV ejection fraction ($R=0.478$; $P=0.0029$), stroke volume ($R=0.316$; $P=0.0440$), and cardiac output ($R=0.398$; $P=0.0098$). A negative relationship was also noticed between total vorticity and mPAP ($R=-0.408$; $P=0.0309$), and a strong positive relationship was noticed with the RAC ($R=0.577$; $P<0.0001$).

Last, to evaluate the diagnostic potential of the noninvasively derived 4D-Flow measures, we performed receiver operating characteristic curve analysis on vorticity and helicity measures (Figure 6). Total helicity revealed the best diagnostic potential from all considered noninvasive markers, with area under the curve value of 0.937, 90.0% sensitivity, 88.9% specificity, and cutoff value of 75.2 $m/s^2$. Vorticity provided considerable area under the curve value of 0.828, 80.0% sensitivity, 79.2% specificity, and cutoff value of 7691 1/s. In comparison, the best CMR-derived parameter for diagnostic evaluation was VVCR, with area under the curve value of 0.870, 80.0% sensitivity, 88.5% specificity, and cutoff value of 0.72.

## Discussion

In this study, we have shown that 4D-Flow CMR quantitative hemodynamic markers reflective of flow turbulence are significantly different in patients with PH and are strongly correlated with the RV metrics of afterload and function. Specifically, we found that reduced helicity and vorticity are reflective of both increased pulmonary stiffness and compromised VVCR, metrics that are increasingly recognized as prognostic markers in PH.[34,35] Our comprehensive report

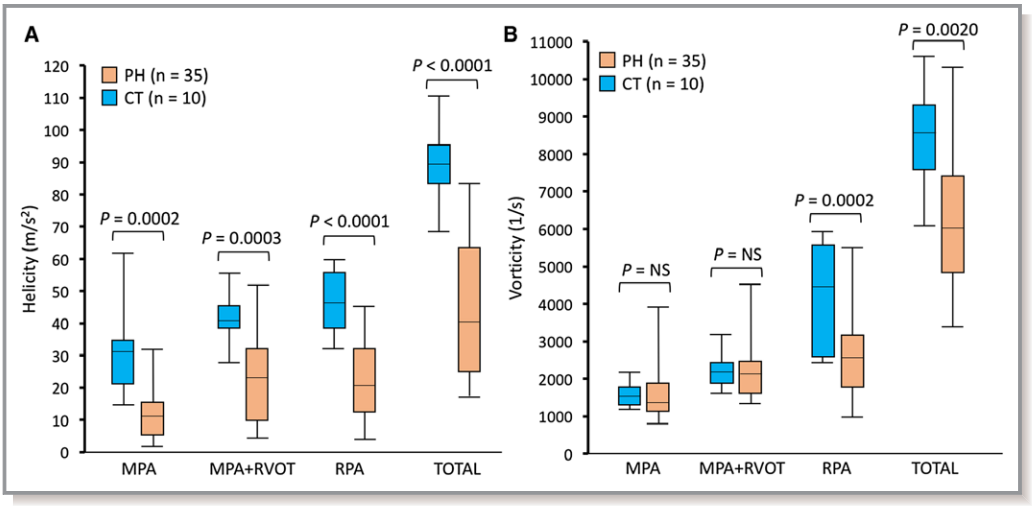


**Figure 4.** Comparison of helicity and vorticity metric measured at different proximal pulmonary arterial compartments. Helicity was significantly reduced in the pulmonary hypertension (PH) group in all considered regions (A), whereas vorticity was significantly reduced in the same group only in the right pulmonary artery (RPA) and when summarized over the entire considered vascular domain (B). CT indicates control; MPA, main pulmonary artery; NS, not significant; and RVOT, right ventricular outflow tract.

**Table 3.** Associations Between Helicity/Vorticity and PH Markers

| PH Markers | Helicity | Vorticity |
|---|---|---|
| EF | 0.865 (<0.0001) | 0.478 (0.0029) |
| VVCR | −0.916 (<0.0001) | −0.426 (0.0058) |
| ESV | −0.482 (0.0008) | −0.190 (0.233) |
| EDV | −0.472 (0.0010) | −0.216 (0.174) |
| SV | 0.477 (0.0009) | 0.316 (0.0440) |
| CO | 0.581 (<0.0001) | 0.398 (0.0098) |
| mPAP | −0.584 (0.0008) | −0.408 (0.0309) |
| MPA-RAC | 0.789 (<0.0001) | 0.577 (<0.0001) |

Correlations are reported as $R/\rho$ values, with corresponding adjusted $P$ values in parentheses. CO indicates cardiac output; EDV, end-diastolic volume; EF, ejection fraction; ESV, end-systolic volume; MPA, main pulmonary artery; mPAP, main pulmonary arterial pressure; PH, pulmonary hypertension; RAC, relative area change; SV, stroke volume; and VVCR, ventricular/vascular coupling ratio.

on quantitative flow hemodynamic indexes in pulmonary circulation indicates the feasibility of this technique for the patient population with PH.

## Quantitative and Qualitative Flow Imaging

Previous reports considering 4D-Flow MRI characterization of PH focused on flow shear hemodynamics or qualitative descriptions of flow formations.[3,4,14,36] Studies investigating shear hemodynamics observed dramatically reduced wall shear stress in the MPA and primary pulmonary arterial branches, along with reduced flow and distended vasculature.[14,36] From the flow hemodynamics point of view, these results correspond to findings described by Reiter et al, who found increased recirculation and large vortex formation along the inferior curvature of the MPA.[3,15] Formations of large-scale vortices in the MPA seem to be a result of vessel dilation and compromised RV function, creating shear layers with dramatically different velocities, resulting in chaotic flow and vortex formations. 4D-Flow MRI enables 3D visualization of these complex flow formations but is majorly limited by high temporal resolution and can be qualitatively prone to subjective grading. We previously applied quantitative spatial hemodynamics to characterize the diastolic dysfunction in patients with PH and chronic obstructive pulmonary disease,

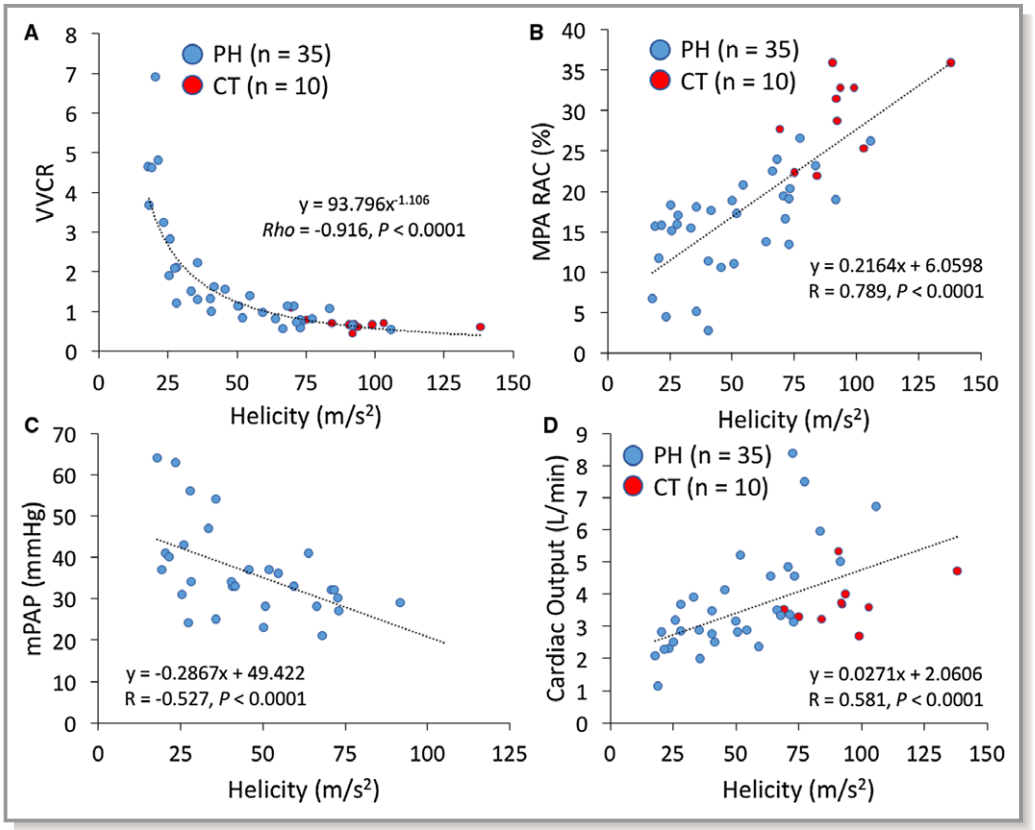


**Figure 5.** The significant correlations between total helicity and right ventricular (RV) afterload/function metrics. A, The significant correlation existed, with ventricular/vascular coupling ratio (VVCR) revealing a negative curvilinear relationship. B, Additional significant association existed with marker of vascular stiffness relative area change (RAC) measured in main pulmonary artery (MPA). C, Total helicity further correlated negatively with the catheterization-derived main pulmonary arterial pressure (mPAP). D, The RV cardiac output correlated positively with helicity, suggesting the supporting role of flow strength in developing high helicity. CT indicates control; and PH, pulmonary hypertension.

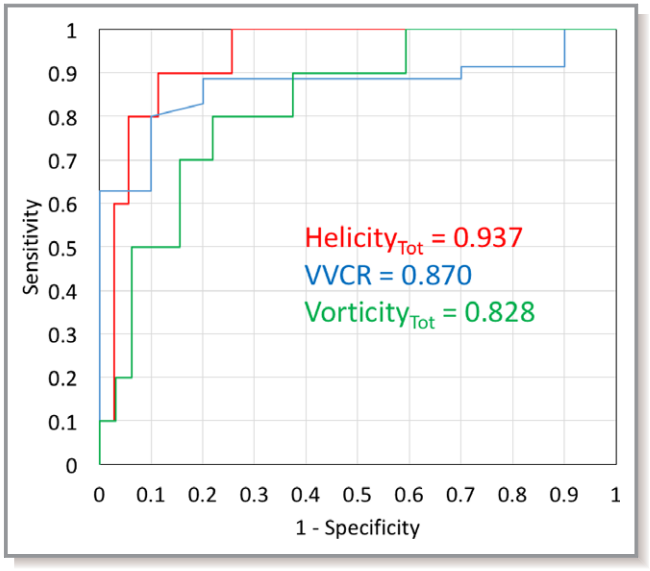


**Figure 6.** The receiver operating characteristic curve analysis of 4-dimensional flow quantitative metrics. Helicity performed better than standard steady-state free precession cardiac magnetic resonance imaging (CMR) metrics. Ventricular/vascular coupling ratio (VVCR) presented the highest area under the curve from all standard CMR markers.

and found that vorticity is a sensitive marker of ventricular stiffness.[29,37,38] Kheyfets et al characterized, for the first time, vorticity in the MPA and found strong negative association between vorticity in the MPA and pulmonary vascular resistance.[4] Counterintuitive results of our and previous studies observing reduced vorticity and helicity stem from the common misconception between qualitative flow markers (ie, vortex formation time and strength grading) and quantitative spatial hemodynamic markers (ie, helicity and vorticity). Both helicity and vorticity are proportional to the strength of the flow and its cohesiveness. Therefore, chaotic and turbulent flow would decrease both parameters, indicating that spatial flow hemodynamic derivatives are reflective of the propagation and stability of laminar flow.[30–32] The contrast between qualitative and quantitative hemodynamic metrics characterizing flow formation can be viewed in Figure 7. It is further apparent that 2 similarly appearing vortices formed in the MPA may have considerably different vorticity. However, additional studies focusing specifically on comparison of qualitative and quantitative flow hemodynamics will have to be performed to address the exact relationship and application of both metrics towards common pathophysiological characteristics.

## Flow and Pulmonary Vascular Remodeling

Turbulent and chaotic flow has, in the past, been strongly correlated with arterial wall remodeling, endothelial dysfunction, inflammation, and vascular stiffness.[8,39] Chaotic and unsteady flow is usually associated with a highly oscillatory and low wall shear stress pattern, which is known to stimulate local inflammation and vessel remodeling. Although the low and oscillatory shear mediates remodeling by means of mechanotransduction by stimulating endothelial surface receptors, chaotic and turbulent flow formations promote prolonged contact time with the endothelium, allowing for granulocyte infiltration, further mediating local inflammation processes.[8,40,41] These processes may then further promote proximal vascular stiffening and, consequently, RV afterload.[9,42] In this study, we found strong correlations between helicity and reduced MPA RAC, already recognized as a component of PH progression and a clinically prognostic marker.[43,44] The most impressive correlation was found between the maximum helicity and the RV VVCR. Noninvasively derived RV-specific ventricular-vascular coupling is subjected to simplifying assumptions, yet still reflective of RV contractility and proximal pulmonary arterial elastance; therefore, it shows energetic transfer between ventricular and arterial compartments.[45] Helicity is reflective of energy dissipation and flow stability.[30,32] Therefore, we speculate that observed flow hemodynamic changes in PH are attributable to both compromised RV contractile function and proximal vascular stiffness, limiting efficient flow conduction to distal pulmonary arteries. This phenomenon would itself elevate the RV afterload and limit efficient lung perfusion. However, more discrete flow hemodynamic studies involving computational fluid dynamics will be required to investigate the relationship between specific flow and mechanical components. Last, VVCR provides a wider physiological range of values than its standardly applied transform-RV ejection fraction, possibly strengthening our observed correlations.[46]

## Flow Hemodynamics in PH Diagnosis

The clinical outcomes and overall prognosis in PH are highly dependent on timely and accurate diagnosis, therefore placing much emphasis on noninvasive and clinically feasible characterization.[47] Although the 4D-Flow MRI is still a relatively novel technique, continual developments in faster postprocessing algorithms already make this technique an attractive tool for preoperative planning and follow-up in variety of aortopathies.[7,13,48] Recently, Swift et al reported a comprehensive prognostic study on patients with a heterogeneous PH cause and found strong prognostic value in using a multivariate model based on applying standard RV MRI metrics.[49] The same group has previously reported the significant prognostic potential of adjusted MRI metrics independently of invasive catheterization metrics in patients with idiopathic PH.[35] Furthermore, combined MRI metrics have strongly correlated with pulmonary pressure and

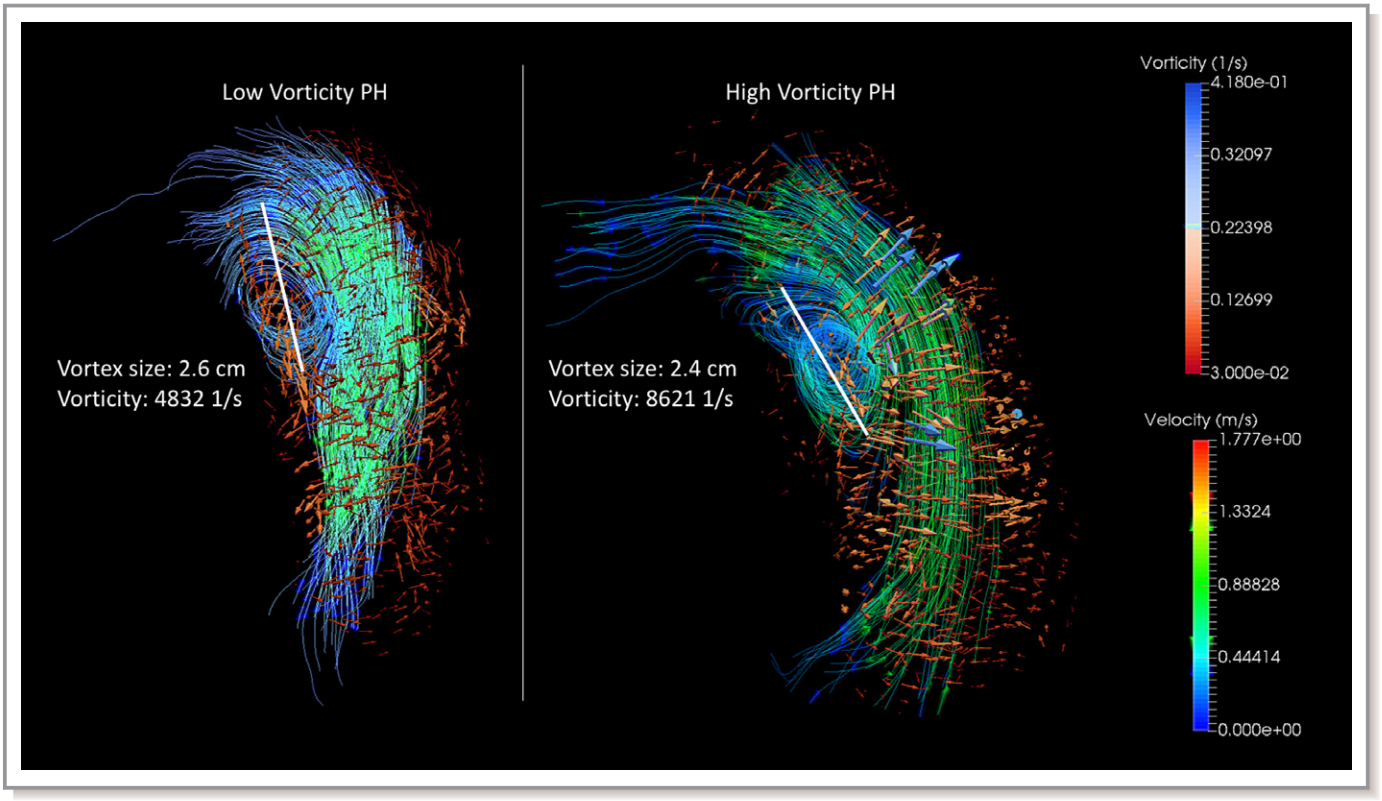


**Figure 7.** Contrast between qualitative and quantitative grading of pulmonary flow hemodynamic patterns. Although both pulmonary hypertension (PH) cases show similar vortex size and flow strength (velocity), the subject on the right reveals dramatically increased vorticity. Anatomically standardized quantitative flow metrics may be then more sensitive for assessment of flow disturbances observed in patients with PH.

resistance, indicating that MRI can be applied as a noninvasive potential diagnostic and serial follow-up tool in patients with PH.[11] 4D-Flow MRI derived vortex existence time, described by Reiter et al, provided, in a blinded prospective study, a diagnostic sensitivity of 100% and a specificity of 91%.[3] In this study, we have attempted to evaluate the diagnostic potential of complex flow hemodynamics and found that helicity and vorticity both correlate with mPAP and that helicity has a higher diagnostic accuracy when compared with standard MRI measures. Given that patients in both aforementioned studies had mild-to-moderate PH per catheterization indexes, we speculate that a comprehensive 4D-Flow MRI evaluation could have an important role in the screening process during the early stage of the disease. However, a larger patient cohort and follow-up study with patients of unified PH cause will be required for detailed diagnostic and prognostic evaluation.

We recognize several limitations in our study. First, the arborization pattern of the RPA may significantly differ in individual patients, making vorticity and helicity normalization with respect to vessel character a challenging task and potentially introducing a computation error. For example, some patients presented branching into combined upper-middle and lower RPAs immediately after MPA bifurcation, whereas most patients presented a more standard pattern, with the upper right pulmonary lobe arterial branch rising within 5 cm from the MPA bifurcation with a distally positioned middle and lower lobe arterial branching point. Potential analysis of the left pulmonary artery would be associated with a similar challenge, along with a significant increase in scanning time given extension of the acquisition window. Second acknowledge that 4D-Flow MRI data sets are associated with low spatiotemporal resolution; therefore, computation of flow/velocity derivatives (wall shear stress, vorticity, and helicity) can be associated with significant analytical error.[24,50] The error propagation analysis associated with 4D-Flow MRI data sets is a complex process involving multifactorial variables, including signal (velocity)/noise ratio, vessel radius, number of cardiac phases, average voxel size, and even strength of the magnetic field. We attempted to mitigate the error analysis by maintaining the identical imaging and postprocessing protocol for every considered case.

Third, we included patients with different PH causes and, therefore, different pathophysiologic components. However, the subgroup analysis among different PH groups failed to show any differences in variability analysis. The receiver operating characteristic curve analysis assessing the

diagnostic potential of quantitative 4D-Flow metrics did not consider patients with suspected/presumptive PH, and will require larger prospective randomized diagnostic analysis. Finally, the catheterization-derived indexes were not obtained in all patients within a single calendar day, potentially limiting associations with invasive catheterization metrics.

## Conclusions

The flow hemodynamic character in patients with PH assessed via quantitative analysis is dramatically different when compared with healthy and normotensive controls. Helicity and vorticity are associated with pulmonary artery stiffness and reduced RV performance. A strong association between helicity in proximal pulmonary arteries and ventricular-vascular coupling suggests that quantitative flow hemodynamic indexes are similarly linked to both ventricular contractile performance and afterload component, represented by proximal pulmonary arterial stiffness. Helicity further presented strong diagnostic potential and implies that flow hemodynamic characterization may become an important component of patient initial and follow-up evaluation. Further longitudinal studies will be required to assess the role of altered flow patterns on vascular remodeling and their prognostic potential in patients with PH.

## Disclosures

None.

## References


1. Freed BH, Collins JD, François CJ, Barker AJ, Cuttica MJ, Chesler NC, Markl M, Shah SJ. MR and CT imaging for the evaluation of pulmonary hypertension. *JACC Cardiovasc Imaging*. 2016;9:715–732.
2. Rodriguez Muñoz D, Markl M, Moya Mur JL, Barker A, Fernández-Golfín C, Lancellotti P, Zamorano Gómez JL. Intracardiac flow visualization: current status and future directions. *Eur Heart J Cardiovasc Imaging*. 2013;14:1029–1038.
3. Reiter G, Reiter U, Kovacs G, Kainz B, Schmidt K, Maier R, Olschewski H, Rienmueller R. Magnetic resonance-derived 3-dimensional blood flow patterns in the main pulmonary artery as a marker of pulmonary hypertension and a measure of elevated mean pulmonary arterial pressure. *Circ Cardiovasc Imaging*. 2008;1:23–30.
4. Kheyfets VO, Schafer M, Podgorski CA, Schroeder JD, Browning J, Hertzberg J, Buckner JK, Hunter KS, Shandas R, Fenster BE. 4D magnetic resonance flow imaging for estimating pulmonary vascular resistance in pulmonary hypertension. *J Magn Reson Imaging*. 2016;44:914–922.
5. Galiè N, Humbert M, Vachiéry J-L, Gibbs S, Lang I, Torbicki A, Simonneau G, Peacock A, Vonk-Noordegraaf A, Beghetti M, Ghofrani A, Gomez Sanchez MA, Hansmann G, Klepetko W, Lancellotti P, Matucci M, McDonagh T, Pierard LA, Trindade PT, Zompatori M, Hoeper M. 2015 ESC/ERS guidelines for the diagnosis and treatment of pulmonary hypertension. *Eur Heart J*. 2015;37:67–119.
6. Szulcek R, Happé CM, Rol N, Fontijn RD, Dickhoff C, Hartemink KJ, Grünberg K, Tu L, Timens W, Nossent GD, Paul MA, Leyen TA, Horrevoets AJ, de Man FS, Guignabert C, Yu PB, Vonk-Noordegraaf A, van Nieuw Amerongen GP, Bogaard HJ. Delayed microvascular shear-adaptation in pulmonary arterial hypertension: role of PECAM-1 cleavage. *Am J Respir Crit Care Med*. 2016;33:1–58.
7. Guzzardi DG, Barker AJ, van Ooij P, Malaisrie SC, Puthumana JJ, Belke DD, Mewhort HEM, Svystonyuk DA, Kang S, Verma S, Collins J, Carr J, Bonow RO, Markl M, Thomas JD, McCarthy PM, Fedak PWM. Valve-related hemodynamics mediate human bicuspid aortopathy. *J Am Coll Cardiol*. 2015;66:892–900.
8. Davies PF. Hemodynamic shear stress and the endothelium in cardiovascular pathophysiology. *Nat Clin Pract Cardiovasc Med*. 2009;6:16–26.
9. Schäfer M, Myers C, Brown RD, Frid MG, Tan W, Hunter K, Stenmark KR. Pulmonary arterial stiffness: toward a new paradigm in pulmonary arterial hypertension pathophysiology and assessment. *Curr Hypertens Rep*. 2016;18:4.
10. Sanz J, Kariisa M, Dellegrottaglie S, Prat-González S, Garcia MJ, Fuster V, Rajagopalan S. Evaluation of pulmonary artery stiffness in pulmonary hypertension with cardiac magnetic resonance. *JACC Cardiovasc Imaging*. 2009;2:286–295.
11. Swift AJ, Rajaram S, Hurdman J, Hill C, Davies C, Sproson TW, Morton AC, Capener D, Elliot C, Condliffe R, Wild JM, Kiely DG. Noninvasive estimation of PA pressure, flow, and resistance with CMR imaging: derivation and prospective validation study from the ASPIRE registry. *JACC Cardiovasc Imaging*. 2013;6:1036–1047.
12. Foris V, Kovacs G, Tscherner M, Olschewski A, Olschewski H. Biomarkers in pulmonary hypertension: what do we know? *Chest*. 2013;144:274–283.
13. Dyverfeldt P, Bissell M, Barker AJ, Bolger AF, Carlhäll C-J, Ebbers T, Francios CJ, Frydrychowicz A, Geiger J, Giese D, Hope MD, Kilner PJ, Kozerke S, Myerson S, Neubauer S, Wieben O, Markl M. 4D flow cardiovascular magnetic resonance consensus statement. *J Cardiovasc Magn Reson*. 2015;17:72.
14. Schafer M, Kheyfets VO, Schroeder JD, Dunning J, Shandas R, Buckner JK, Browning J, Hertzberg J, Hunter KS, Fenster BE. Main pulmonary arterial wall shear stress correlates with invasive hemodynamics and stiffness in pulmonary hypertension. *Pulm Circ*. 2016;6:37–45.
15. Reiter U, Reiter G, Kovacs G, Stalder AF, Gulsun MA, Greiser A, Olschewski H, Fuchsjäger M. Evaluation of elevated mean pulmonary arterial pressure based on magnetic resonance 4D velocity mapping: comparison of visualization techniques. *PLoS One*. 2013;8:1–9.
16. Binter C, Gotschy A, Sündermann SH, Frank M, Tanner FC, Lüscher TF, Manka R, Kozerke S. Turbulent kinetic energy assessed by multipoint 4-dimensional flow magnetic resonance imaging provides additional information relative to echocardiography for the determination of aortic stenosis severity. *Circ Cardiovasc Imaging*. 2017;10:e005486.
17. Barker AJ, Markl M, Bürk J, Lorenz R, Bock J, Bauer S, Schulz-Menger J, von Knobelsdorff-Brenkenhoff F. Bicuspid aortic valve is associated with altered wall shear stress in the ascending aorta. *Circ Cardiovasc Imaging*. 2012;5:457–466.
18. Gallo D, Steinman DA, Bijari PB, Morbiducci U. Helical flow in carotid bifurcation as surrogate marker of exposure to disturbed shear. *J Biomech*. 2012;45:2398–2404.
19. Lorenz R, Bock J, Barker A, von Knobelsdorff-Brenkenhoff F, Vrints CJM, Korvink JG, Bissell MM, Schulz-Menger J, Markl M. 4D flow magnetic resonance imaging in bicuspid aortic valve disease demonstrates altered distribution of aortic blood flow helicity. *Magn Reson Med*. 2014;71:1542–1553.
20. Jiang YZ, Manduchi E, Jimenez JM, Davies PF. Endothelial epigenetics in biomechanical stress: disturbed flow-mediated epigenomic plasticity in vivo and in vitro. *Arterioscler Thromb Vasc Biol*. 2015;35:1317–1326.
21. Schäfer M, Ivy DD, Barker AJ, Kheyfets V, Shandas R, Abman SH, Hunter KS, Truong U. Characterization of CMR-derived haemodynamic data in children with pulmonary arterial hypertension. *Eur Heart J Cardiovasc Imaging*. 2016;18:424–431.
22. Sanz J, García-Alvarez A, Fernández-Friera L, Nair A, Mirelis JG, Sawit ST, Pinney S, Fuster V. Right ventriculo-arterial coupling in pulmonary hypertension: a magnetic resonance study. *Heart*. 2012;98:238–243.
23. Bock J, Markl M, Kreher B, Henning J. Optimized pre-processing of time-resolved 2D and 3D phase contrast MRI data. *Proceedings 15th Annual Meeting ISMRM*. Berlin, Germany: 2007:Abstract 3138.
24. Stalder AF, Russe MF, Frydrychowicz A, Bock J, Hennig J, Markl M. Quantitative 2D and 3D phase contrast MRI: optimized analysis of blood flow and vessel wall parameters. *Magn Reson Med*. 2008;60:1218–1231.
25. Garcia J, Barker AJ, Murphy I, Jarvis K, Schnell S, Collins JD, Carr JC, Malaisrie SC, Markl M. Four-dimensional flow magnetic resonance imaging-based characterization of aortic morphometry and haemodynamics: impact of age, aortic diameter, and valve morphology. *Eur Heart J Cardiovasc Imaging*. 2015;7:877–884.
26. Truong U, Fonseca B, Dunning J, Burgett S, Lanning C, Ivy DD, Shandas R, Hunter K, Barker AJ. Wall shear stress measured by phase contrast cardiovascular magnetic resonance in children and adolescents with pulmonary arterial hypertension. *J Cardiovasc Magn Reson*. 2013;15:81.
27. Fenster BE, Browning J, Schroeder JD, Schafer M, Podgorski CA, Smyser J, Silveira LJ, Buckner JK, Hertzberg JR. Vorticity is a marker of right ventricular diastolic dysfunction. *Am J Physiol Heart Circ Physiol*. 2015;309:H1087–H1093.

28. Browning J, Hertzberg J, Schroeder J, Fenster B. 4D flow assessment of vorticity in right ventricular diastolic dysfunction. *Bioengineering (Basel)*. 2017;4:30.
29. Schäfer M, Humphries S, Stenmark KR, Kheyfets VO, Buckner JK, Hunter KS, Fenster BE. 4D-flow cardiac magnetic resonance-derived vorticity is sensitive marker of left ventricular diastolic dysfunction in patients with mild-to-moderate chronic obstructive pulmonary disease. *Eur Heart J Cardiovasc Imaging*. 2017. https://academic.oup.com/ehjcimaging/article-abstract/doi/10.1093/ehjci/jex069/3778269?redirectedFrom=fulltext. DOI: 10.1093/ehjci/jex069. Accessed November 1, 2001.
30. Morbiducci U, Ponzini R, Grigioni M, Redaelli A. Helical flow as fluid dynamic signature for atherogenesis risk in aortocoronary bypass: a numeric study. *J Biomech*. 2007;40:519–534.
31. Morbiducci U, Ponzini R, Rizzo G, Cadioli M, Esposito A, De Cobelli F, Del Maschio A, Montevecchi FM, Redaelli A. In vivo quantification of helical blood flow in human aorta by time-resolved three-dimensional cine phase contrast magnetic resonance imaging. *Ann Biomed Eng*. 2009;37:516–531.
32. Moffatt HK. The degree of knottedness of tangled vortex lines. *J Fluid Mech*. 1969;35:117.
33. Moffatt H, Tsinober A. Helicity in laminar and turbulent flow. *Annu Rev Fluid Mech*. 1992;24:281–312.
34. Vanderpool RR, Pinsky MR, Naeije R, Deible C, Kosaraju V, Bunner C, Mathier MA, Lacomis J, Champion HC, Simon MA. RV-pulmonary arterial coupling predicts outcome in patients referred for pulmonary hypertension. *Heart*. 2015;101:37–43.
35. Swift AJ, Rajaram S, Campbell MJ, Hurdman J, Thomas S, Capener D, Elliot C, Condliffe R, Wild JM, Kiely DG. Prognostic value of cardiovascular magnetic resonance imaging measurements corrected for age and sex in idiopathic pulmonary arterial hypertension. *Circ Cardiovasc Imaging*. 2014;7:100–106.
36. Barker AJ, Roldán-Alzate A, Entezari P, Shah SJ, Chesler NC, Wieben O, Markl M, François CJ. Four-dimensional flow assessment of pulmonary artery flow and wall shear stress in adult pulmonary arterial hypertension: results from two institutions. *Magn Reson Med*. 2014;73:1904–1913.
37. Fenster B, Podgorski CA, Schroeder JD, Lin B, Reisner SD, Browning J, Hertzberg JR, Buckner KJ, Schafer M. Left ventricular vorticity is marker of ventricular interdependency in pulmonary arterial hypertension. *J Cardiovasc Magn Reson*. 2015;17:P14.
38. Schäfer M, Browning J, Schroeder JD, Shandas R, Kheyfets VO, Buckner JK, Hunter KS, Fenster BE. Vorticity is a marker of diastolic ventricular interdependency in pulmonary hypertension. *Pulm Circ*. 2016;6:46–54.
39. Hassoun PM, Mouthon L, Barberà JA, Eddahibi S, Flores SC, Grimminger F, Jones PL, Maitland ML, Michelakis ED, Morrell NW, Newman JH, Rabinovitch M, Schermuly R, Stenmark KR, Voelkel NF, Yuan JXJ, Humbert M. Inflammation, growth factors, and pulmonary vascular remodeling. *J Am Coll Cardiol*. 2009;54:S10–S19.
40. Malek AM, Alper SL, Izumo S. Hemodynamic shear stress and its role in atherosclerosis. *JAMA*. 1999;282:2035–2042.
41. Huveneers S, Daemen MJAP, Hordijk PL. Between Rho(k) and a hard place: the relation between vessel wall stiffness, endothelial contractility, and cardiovascular disease. *Circ Res*. 2015;116:895–908.
42. Tan W, Madhavan K, Hunter KS, Park D, Stenmark KR. Vascular stiffening in pulmonary hypertension: cause or consequence? (2013 Grover Conference series). *Pulm Circ*. 2014;4:560–580.
43. Swift AJ, Rajaram S, Condliffe R, Capener D, Hurdman J, Elliot C, Kiely DG, Wild JM. Pulmonary artery relative area change detects mild elevations in pulmonary vascular resistance and predicts adverse outcome in pulmonary hypertension. *Invest Radiol*. 2012;47:571–577.
44. Swift AJ, Wild JM, Nagle SK, Roldan-Alzate A, Francois CJ, Fain S, Johnson K, Capener D, van Beek EJ, Kiely DG, Wang K, Schiebler ML. Quantitative magnetic resonance imaging of pulmonary hypertension: a practical approach to the current state of the art. *J Thorac Imaging*. 2014;29:68–79.
45. Vonk Noordegraaf A, Westerhof BE, Westerhof N. The relationship between the right ventricle and its load in pulmonary hypertension. *J Am Coll Cardiol*. 2017;69:236–243.
46. Vanderpool RR, Rischard F, Naeije R, Hunter K, Simon MA. Simple functional imaging of the right ventricle in pulmonary hypertension: can right ventricular ejection fraction be improved? *Int J Cardiol*. 2016;223:93–94.
47. Sutendra G, Michelakis ED. Pulmonary arterial hypertension: challenges in translational research and a vision for change. *Sci Transl Med*. 2013;5:208sr5.
48. Hope TA, Kvitting JPE, Hope MD, Miller DC, Markl M, Herfkens RJ. Evaluation of Marfan patients status post valve-sparing aortic root replacement with 4D flow. *Magn Reson Imaging*. 2013;31:1479–1484.
49. Swift AJ, Capener D, Johns C, Hamilton N, Rothman A, Elliot C, Condliffe R, Charalampopoulos A, Rajaram S, Lawrie A, Campbell MJ, Wild JM, Kiely DG. Magnetic resonance imaging in the prognostic evaluation of patients with pulmonary arterial hypertension. *Am J Respir Crit Care Med*. 2017;196:228–239.
50. Hess AT, Bissell MM, Ntusi NAB, Lewis AJM, Tunnicliffe EM, Greiser A, Stalder AF, Francis JM, Myerson SG, Neubauer S, Robson MD. Aortic 4D flow: quantification of signal-to-noise ratio as a function of field strength and contrast enhancement for 1.5T, 3T, and 7T. *Magn Reson Med*. 2015;73:1864–1871.

# SUPPLEMENTAL MATERIAL

**Figure S1**. Bland-Altman graphical representation of inter- and intra- observer agreement analysis for helicity computation in RV outflow tract – MPA conduit. **A**) Interobserver analysis in control cases revealed the mean difference -0.4 m/s/s (red solid line) with narrow gap between upper and lower 95% confident intervals (red dashed lines). **B**) Good agreement also existed in helicity measurement in PH population with the mean difference of 0.4 m/s/s. **C**) and **D**) Intraobserver agreement assessed in 6 months period revealed very good agreement for both control and PH groups.